Application of Least-Squares Adjustment Technique to Geometric Camera Calibration and Photogrammetric Flow Visualization

Fang-Jenq Chen
Senior Research Engineer
NASA Langley Research Center
Hampton, Virginia 23681-0001

KEYWORDS

Flow Visualization, Photogrammetry, Camera Calibration, Image Processing

Submitted for
ISA 43rd International Instrumentation Symposium
May 4-8, 1997, Orlando, Florida

Application of Least-Squares Adjustment Technique to Geometric Camera Calibration and Photogrammetric Flow Visualization

Fang-Jenq Chen
Senior Research Engineer
NASA Langley Research Center
Hampton, Virginia 23681-0001

KEYWORDS

Flow Visualization, Photogrammetry, Camera Calibration, Image Processing

ABSTRACT

Flow visualization produces data in the form of two-dimensional images. If the optical components of a camera system are perfect, the transformation equations between the two-dimensional image and the three-dimensional object space are linear and easy to solve. However, real camera lenses introduce nonlinear distortions that affect the accuracy of transformation unless proper corrections are applied. An iterative least-squares adjustment algorithm is developed to solve the nonlinear transformation equations incorporated with distortion corrections. Experimental applications demonstrate that a relative precision on the order of 40,000 is achievable without tedious laboratory calibrations of the camera.

1. INTRODUCTION

The photogrammetric technique was originally developed to determine topography using aerial photography with "metric" cameras. Due to the advent of CCD (Charge-Couple Device) digital cameras, non-topographic applications of photogrammetry especially in the field of close-range photogrammetry have become increasingly important.

A simple method for close-range photogrammetric data reduction with non-metric cameras was developed by Abdel-Aziz and Karara.[1] It establishes the Direct Linear Transformation (DLT) between the coordinates of image points, measured with a comparator, and the corresponding object-space coordinates. Since the DLT is a linear approach, it neglects nonlinear distortions introduced by real camera lenses. Several methods exist for geometric calibration of cameras. The most accurate approach is to perform a laboratory calibration as described by Snow et al.[2] This is a time-consuming process and requires specially fabricated test objects. A more convenient method is the in-situ calibration suggested by Bopp and Krauss,[3] in which the effects of distortion are determined together with other parameters of transformation by solving a set of nonlinear equations. The drawback of the in-situ calibration is that the solution may fail to converge to the best answer. A third possibility is a hybrid approach proposed by Cattafesta and Moore,[4] which applies the results of a less rigorous laboratory calibration to the in-situ calibration to improve the likelihood of a good answer.

An algorithm using an iterative least-squares adjustment scheme has been developed to solve the nonlinear equations of the in-situ or hybrid calibration. This algorithm requires less CPU time to achieve the same level of accuracy in solutions as compared to the Levenberg-Marquardt algorithm used by other investigators.[4] Practical tests of these algorithms are conducted with luminescent temperature-sensitive paint (TSP) imaging on a three-dimensional swept-wing model tested in the Supersonic Low-Disturbance Tunnel at NASA Langley.

2. MATHEMATICAL FORMULATION

In the absence of distortion, the Direct Linear Transformation (DLT)[1] between a point (X,Y,Z) in object space and its corresponding image space coordinates (x,y) can be expressed by the linear fractional equations

$$x = \frac{L_1X + L_2Y + L_3Z + L_4}{L_9X + L_{10}Y + L_{11}Z + 1} \qquad \text{and} \qquad y = \frac{L_5X + L_6Y + L_7Z + L_8}{L_9X + L_{10}Y + L_{11}Z + 1} \tag{1}$$

These equations are based on the collinearity condition that the object point, perspective center of the lens, and ideal image point all lie on a straight line. Eqns. (1) can be solved directly for the 11 transformation parameters L_1 L L_{11} if there are at least six registration marks in the image whose object-space coordinates are known.

Optical distortion of imperfect cameras will cause the image point to fall in a slightly different location. Figure 1 shows a schematic of the image geometry with distortion. To reestablish collinearity, correction terms Δx and Δy are added to Eqns. (1):

$$x + \Delta x = \frac{L_1X + L_2Y + L_3Z + L_4}{L_9X + L_{10}Y + L_{11}Z + 1}$$

$$y + \Delta y = \frac{L_5X + L_6Y + L_7Z + L_8}{L_9X + L_{10}Y + L_{11}Z + 1} \tag{2}$$

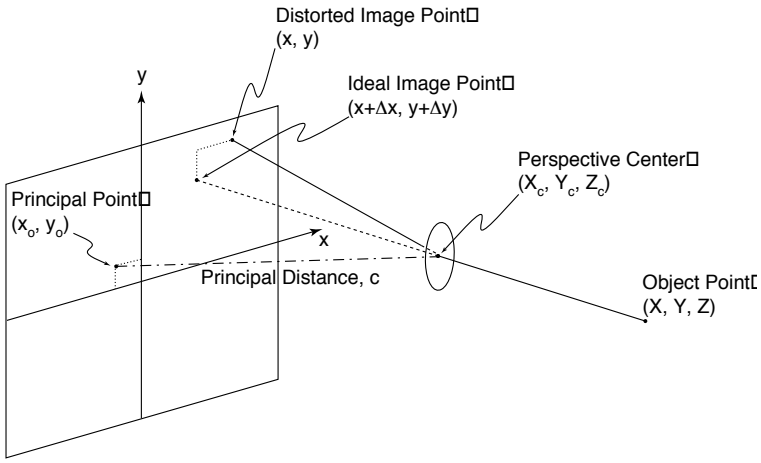

Figure 1. - Image geometry with distortion.

Considering lens distortions,[5] there are three symmetric parameters (K_1,K_2,K_3) for radial distortion and two asymmetric parameters (P_1,P_2) for decentering distortion. In addition, two more affinity parameters (A_1,A_2) to account for non-orthogonality and differential scaling of the sensor axes are very applicable to CCD cameras. The cumulative influence of these distortions can be expressed as

$$\begin{aligned}\Delta x &= x'\left(K_1r^2 + K_2r^4 + K_3r^6\right) + P_1\left(r^2 + 2x'^2\right) + 2P_2x'y' \\ \Delta y &= y'\left(K_1r^2 + K_2r^4 + K_3r^6\right) + 2P_1x'y' + P_2\left(r^2 + 2y'^2\right) + A_1x' + A_2y'\end{aligned} \tag{3}$$

where (x',y') is the location of the distorted image point relative to the principal point (x_0,y_0):

$$x' = x - x_0 \qquad \text{and} \qquad y' = y - y_0 \tag{4}$$

and r is the radial distance of the distorted image point from the principal point:

$$r^2 = x'^2 + y'^2 \tag{5}$$

As shown in Figure 1, the optical axis of the lens is defined by the line perpendicular to the image plane that passes through the perspective center (X_c,Y_c,Z_c). The intersection point of the optical axis with the image plane is called the principal point that is not necessarily located at the geometric center of the image, although it is usually in this vicinity. The distance from the perspective center to the principal point is

defined as the principal distance c. Note that c equals the focal length of a lens when the object is imaged at infinity.

The transformation between image space and object space has 9 degrees of freedom. Three of these (x_0, y_0, c) specify the interior orientation of the camera. The other six are associated with the exterior orientation of the camera: (X_c, Y_c, Z_c) related to 3 translations and (ω, ϕ, κ) related to 3 rotations with respect to the object-space coordinate axes X, Y, and Z, respectively. Therefore, the 11 transformation parameters $L_1 \sim L_{11}$ have to fulfill the two constraints as noted by Bopp and Krauss[6]

$$\begin{aligned}
&\left(L_1^2 + L_2^2 + L_3^2\right) - \left(L_5^2 + L_6^2 + L_7^2\right) + \frac{\left(L_5L_9 + L_6L_{10} + L_7L_{11}\right)^2 - \left(L_1L_9 + L_2L_{10} + L_3L_{11}\right)^2}{L_9^2 + L_{10}^2 + L_{11}^2} = 0 \\
&L_1L_5 + L_2L_6 + L_3L_7 - \frac{\left(L_1L_9 + L_2L_{10} + L_3L_{11}\right)\left(L_5L_9 + L_6L_{10} + L_7L_{11}\right)}{L_9^2 + L_{10}^2 + L_{11}^2} = 0
\end{aligned} \tag{6}$$

The interior-orientation parameters (x_0, y_0, c) can be computed from the 11 transformation parameters $L_1 \sim L_{11}$ by the following equations[4]

$$\begin{aligned}
x_0 &= \left(L_1L_9 + L_2L_{10} + L_3L_{11}\right) / \left(L_9^2 + L_{10}^2 + L_{11}^2\right) \\
y_0 &= \left(L_5L_9 + L_6L_{10} + L_7L_{11}\right) / \left(L_9^2 + L_{10}^2 + L_{11}^2\right) \\
c_x &= \sqrt{\left(L_1^2 + L_2^2 + L_3^2\right) / \left(L_9^2 + L_{10}^2 + L_{11}^2\right) - x_0^2} \\
c_y &= \sqrt{\left(L_5^2 + L_6^2 + L_7^2\right) / \left(L_9^2 + L_{10}^2 + L_{11}^2\right) - y_0^2} \\
c &= (c_x + c_y)/2
\end{aligned} \tag{7}$$

The exterior-orientation parameters (X_c, Y_c, Z_c) and (ω, ϕ, κ) can be obtained, if desired, using the relations[4]

$$\begin{aligned}
&\begin{bmatrix} X_c \\ Y_c \\ Z_c \end{bmatrix} = -\begin{bmatrix} L_1 & L_2 & L_3 \\ L_5 & L_6 & L_7 \\ L_9 & L_{10} & L_{11} \end{bmatrix}^{-1} \begin{bmatrix} L_4 \\ L_8 \\ 1 \end{bmatrix} \\
&\omega = \tan^{-1}(-L_{10}/L_{11}) \\
&\phi = \sin^{-1}\left(-L_9 \Big/ \sqrt{L_9^2 + L_{10}^2 + L_{11}^2}\right) \\
&\kappa = \cos^{-1}\left((L_1 - x_0L_9) \Big/ \left(c \cdot \cos\phi \cdot \sqrt{L_9^2 + L_{10}^2 + L_{11}^2}\right)\right)
\end{aligned} \tag{8}$$

An iterative least-squares adjustment scheme is developed to solve the 11 transformation parameters $L_1 \sim L_{11}$ and up to 7 correction parameters $(K_1, K_2, K_3, P_1, P_2, A_1, A_2)$, plus the principal point (x_0, y_0) that can be either solved as additional unknowns or computed from the 11 update transformation parameters $L_1 \sim L_{11}$ by Eqns. (7) after each iteration. The algorithm solves a set of nonlinear equations of Eqns. (2), (6) and (7) in the rewritten forms as

$$
\begin{aligned}
f &= x + \Delta x - \frac{L_1 X + L_2 Y + L_3 Z + L_4}{L_9 X + L_{10} Y + L_{11} Z + 1} \\
g &= y + \Delta y - \frac{L_5 X + L_6 Y + L_7 Z + L_8}{L_9 X + L_{10} Y + L_{11} Z + 1} \\
c_1 &= \left(L_1^{\,2} + L_2^{\,2} + L_3^{\,2}\right) - \left(L_5^{\,2} + L_6^{\,2} + L_7^{\,2}\right) + \frac{\left(L_5 L_9 + L_6 L_{10} + L_7 L_{11}\right)^2 - \left(L_1 L_9 + L_2 L_{10} + L_3 L_{11}\right)^2}{L_9^{\,2} + L_{10}^{\,2} + L_{11}^{\,2}} \\
c_2 &= L_1 L_5 + L_2 L_6 + L_3 L_7 - \frac{\left(L_1 L_9 + L_2 L_{10} + L_3 L_{11}\right)\left(L_5 L_9 + L_6 L_{10} + L_7 L_{11}\right)}{L_9^{\,2} + L_{10}^{\,2} + L_{11}^{\,2}} \\
c_3 &= x_0 - \left(L_1 L_9 + L_2 L_{10} + L_3 L_{11}\right) \Big/ \left(L_9^{\,2} + L_{10}^{\,2} + L_{11}^{\,2}\right) \\
c_4 &= y_0 - \left(L_5 L_9 + L_6 L_{10} + L_7 L_{11}\right) \Big/ \left(L_9^{\,2} + L_{10}^{\,2} + L_{11}^{\,2}\right) \\
c_5 &= c - \sqrt{\left(L_1^{\,2} + L_2^{\,2} + L_3^{\,2}\right) \Big/ \left(L_9^{\,2} + L_{10}^{\,2} + L_{11}^{\,2}\right) - x_0^{\,2}} \\
c_6 &= c - \sqrt{\left(L_5^{\,2} + L_6^{\,2} + L_7^{\,2}\right) \Big/ \left(L_9^{\,2} + L_{10}^{\,2} + L_{11}^{\,2}\right) - y_0^{\,2}}
\end{aligned}
\tag{9}
$$

where the first pair of equations are applied to each registration mark that represents the horizontal and vertical distance between the measured (x, y) and the computed (x, y) using the current guesses for the DLT and correction parameters. This produces $2N$ equations for N registration marks. The remaining pairs of equations are defined as the L-constraints for c_1 and c_2, P-constraints for c_3 and c_4, and C-constraints for c_5 and c_6, because these equations represent the constraints to be satisfied by the transformation parameters $L_1 \text{L}\ L_{11}$, the principal point (x_0, y_0), and the principal distance c, respectively. The values of $c_1 \text{L}\ c_6$ are zero when the given constraints are satisfied. In this formulation, the maximum number of equations is $(2N + 6)$ when all constraints are applied, and the maximum number of unknowns is 20, i.e., $(L_1, \text{L}\ , L_{11}, x_0, y_0, K_1, K_2, K_3, P_1, P_2, A_1, A_2)$.

During iteration, the values of the unknowns are updated by adding a small adjustment to each. The adjustments are calculated by finding a least-squares solution to

$$
\begin{bmatrix}
\partial f_1/\partial L_1 & \text{L} & \partial f_1/\partial L_{11} & \partial f_1/\partial x_0 & \partial f_1/\partial y_0 & \partial f_1/\partial K_1 & \partial f_1/\partial K_2 & \partial f_1/\partial K_3 & \partial f_1/\partial P_1 & \partial f_1/\partial P_2 & \partial f_1/\partial A_1 & \partial f_1/\partial A_2 \\
\partial g_1/\partial L_1 & \text{L} & \partial g_1/\partial L_{11} & \partial g_1/\partial x_0 & \partial g_1/\partial y_0 & \partial g_1/\partial K_1 & \partial g_1/\partial K_2 & \partial g_1/\partial K_3 & \partial g_1/\partial P_1 & \partial g_1/\partial P_2 & \partial g_1/\partial A_1 & \partial g_1/\partial A_2 \\
\text{M} & \text{O} & \text{M} & \text{M} & \text{M} & \text{M} & \text{M} & \text{M} & \text{M} & \text{M} & \text{M} & \text{M} \\
\partial f_N/\partial L_1 & \text{L} & \partial f_N/\partial L_{11} & \partial f_N/\partial x_0 & \partial f_N/\partial y_0 & \partial f_N/\partial K_1 & \partial f_N/\partial K_2 & \partial f_N/\partial K_3 & \partial f_N/\partial P_1 & \partial f_N/\partial P_2 & \partial f_N/\partial A_1 & \partial f_N/\partial A_2 \\
\partial g_N/\partial L_1 & \text{L} & \partial g_N/\partial L_{11} & \partial g_N/\partial x_0 & \partial g_N/\partial y_0 & \partial g_N/\partial K_1 & \partial g_N/\partial K_2 & \partial g_N/\partial K_3 & \partial g_N/\partial P_1 & \partial g_N/\partial P_2 & \partial g_N/\partial A_1 & \partial g_N/\partial A_2 \\
\partial c_1/\partial L_1 & \text{L} & \partial c_1/\partial L_{11} & 0 & 0 & 0 & 0 & 0 & 0 & 0 & 0 & 0 \\
\partial c_2/\partial L_1 & \text{L} & \partial c_2/\partial L_{11} & 0 & 0 & 0 & 0 & 0 & 0 & 0 & 0 & 0 \\
\partial c_3/\partial L_1 & \text{L} & \partial c_3/\partial L_{11} & \partial c_3/\partial x_0 & \partial c_3/\partial y_0 & 0 & 0 & 0 & 0 & 0 & 0 & 0 \\
\partial c_4/\partial L_1 & \text{L} & \partial c_4/\partial L_{11} & \partial c_4/\partial x_0 & \partial c_4/\partial y_0 & 0 & 0 & 0 & 0 & 0 & 0 & 0 \\
\partial c_5/\partial L_1 & \text{L} & \partial c_5/\partial L_{11} & \partial c_5/\partial x_0 & \partial c_5/\partial y_0 & 0 & 0 & 0 & 0 & 0 & 0 & 0 \\
\partial c_6/\partial L_1 & \text{L} & \partial c_6/\partial L_{11} & \partial c_6/\partial x_0 & \partial c_6/\partial y_0 & 0 & 0 & 0 & 0 & 0 & 0 & 0
\end{bmatrix}
\begin{bmatrix}
\Delta L_1 \\ \text{M} \\ \Delta L_{11} \\ \Delta x_0 \\ \Delta y_0 \\ \Delta K_1 \\ \Delta K_2 \\ \Delta K_3 \\ \Delta P_1 \\ \Delta P_2 \\ \Delta A_1 \\ \Delta A_2
\end{bmatrix}
= -
\begin{bmatrix}
f_1 \\ g_1 \\ \text{M} \\ f_N \\ g_N \\ c_1 \\ c_2 \\ c_3 \\ c_4 \\ c_5 \\ c_6
\end{bmatrix}
$$

Iteration is stopped when the maximum adjustment falls below a given tolerance. A weight matrix can be included in the least-squares solution to place more or less emphasis on the constraint equations or to account for different uncertainties in the registration-mark locations. Setting the weight of the constraints or the registration-mark locations to zero removes them from the solution. All registration marks and

constraints are weighted equally in this study. Each pair of constraints can also be turned "on" or "off" by control keywords at user's choice.

The principal-point location computed in the solution sometimes tends to large errors. Three techniques have been implemented to deal with this problem. The first one is to bound the principal point within a specified range, but let it vary freely within that range in each iteration. The second technique is to keep the principal point constant, using the value from the initial guess in every iteration. The principal-point constraints can be included in this situation as well, in which case compliance will be sought by adjusting the L values alone, not the principal-point location. In the third technique, the principal point is no longer solved as unknown variables but computed directly from the L values. The expressions for $\partial f_i/\partial L_j$ and $\partial g_i/\partial L_j$ are greatly simplified since Δx and Δy no longer contribute any terms to the partial derivatives with respect to the principal point. To simplify the code, when the originally described method is implemented, partial derivatives are first computed considering x_0 and y_0 to be additional variables. Then the following chain-rule operation is performed:

$$\begin{bmatrix} \partial f_1/\partial L_1 & \cdots & \partial f_1/\partial L_{11} \\ \partial g_1/\partial L_1 & \cdots & \partial g_1/\partial L_{11} \\ \vdots & \ddots & \vdots \\ \partial f_N/\partial L_1 & \cdots & \partial f_N/\partial L_{11} \\ \partial g_N/\partial L_1 & \cdots & \partial g_N/\partial L_{11} \end{bmatrix} \rightarrow \begin{bmatrix} \partial f_1/\partial L_1 & \cdots & \partial f_1/\partial L_{11} \\ \partial g_1/\partial L_1 & \cdots & \partial g_1/\partial L_{11} \\ \vdots & \ddots & \vdots \\ \partial f_N/\partial L_1 & \cdots & \partial f_N/\partial L_{11} \\ \partial g_N/\partial L_1 & \cdots & \partial g_N/\partial L_{11} \end{bmatrix} + \begin{bmatrix} \partial f_1/\partial x_0 & \partial f_1/\partial y_0 \\ \partial g_1/\partial x_0 & \partial g_1/\partial y_0 \\ \vdots & \vdots \\ \partial f_N/\partial x_0 & \partial f_N/\partial y_0 \\ \partial g_N/\partial x_0 & \partial g_N/\partial y_0 \end{bmatrix} \begin{bmatrix} \partial x_0/\partial L_1 & \cdots & \partial x_0/\partial L_{11} \\ \partial y_0/\partial L_1 & \cdots & \partial y_0/\partial L_{11} \end{bmatrix} \tag{10}$$

x_0 and y_0 are then removed from the vector of unknowns and the $\partial/\partial x_0$ and $\partial/\partial y_0$ elements are removed from the matrix of partial derivatives. Of course, the *P*-constraints are not applicable under this situation.

3. PRACTICAL TESTS AND RESULTS

A Photometrics camera (Model TEK512AF) with an AF Micro-Nikkor 60 *mm* f/2.8 lens was used in TSP luminescence imaging of a supersonic swept-wing model. This camera is a scientific-grade, thermoelectrically cooled, 14-bit digital CCD camera. It has a 512 × 512 sensor array with 27 μm square sensor elements. Results of laboratory calibration of this camera were given in Reference 4 and summarized as follows:

$$\begin{aligned} x_0(mm) &= -0.1430 \\ y_0(mm) &= 0.0917 \\ c(mm) &= 63.9537 \\ K_1(1/mm^2) &= -1.392 \times 10^{-5} \\ \Sigma &= 28000 \end{aligned} \tag{11}$$

where Σ is the relative precision. A relative precision of 10,000 implies that 0.1 mm can be resolved in an image spanning 1 m along its diagonal. The higher-order symmetric, asymmetric, and affine distortion parameters were set to zero in this laboratory calibration after initial trials confirmed that they were negligible. Forcing these terms to zero reduces the risk of problems associated with over-parameterization in the calibration results. These laboratory calibration results will be used as a bench mark for comparing the in-situ and hybrid calibrations discussed in the following.

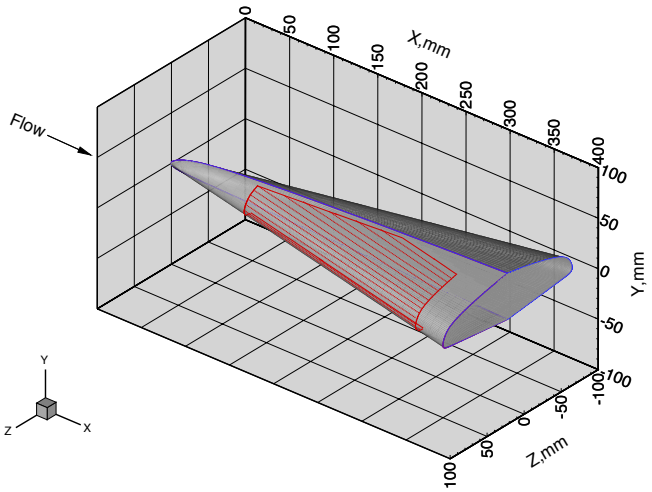

Figure 2. - Swept-wing model with suction panel.

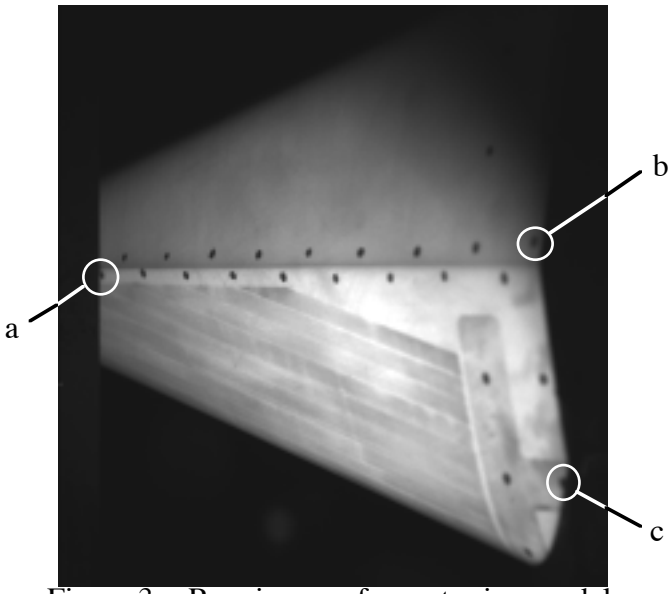

Figure 3. - Raw image of swept-wing model showing 21 targets and 3 check points.

The same CCD camera system with the same lens settings was used for the in-situ and hybrid calibrations with luminescent TSP imaging on a three-dimensional swept-wing model tested in the Supersonic Low-Disturbance Tunnel at NASA Langley. Figure 2 shows a sketch of the swept-wing model partially covered with a suction panel that is denoted by a polygon filled with a group of parallel lines. Details on the tunnel, model and TSP technique were given in Reference 7. The TSP technique is developed for the purpose of transition detection in order to evaluate the Laminar Flow Control technique with surface suction on the swept-wing model. Figure 3 shows an original "raw" image, from which the transition data on the lower half of the model is obtained. Note the locations of the black targets, the object-space centroid locations of which were measured by a Brown and Sharpe Coordinate Measuring Machine in terms of model coordinates. There are 21 targets used as registration marks for camera calibration, and 3 check points denoted as "a", "b" and "c" are reserved for calibration evaluation.

Figure 4 shows a "transition" image of the swept-wing model in Mach 3.5 flow that is from left to right. The long dimension of image covers approximately 340 *mm*. The onset of transition is demarcated in the image by a light-gray parabolic band. To determine the locations of the transition front in model coordinates, various combinations of the photogrammetric techniques described earlier in this paper were used to perform the mapping. Tables 1(a) and 1(b) summarize the results of photogrammetric mapping by the iterative least-squares adjustment algorithm described in the previous section and the Levenberg-Marquardt algorithm used by other investigators,[4] respectively. Four cases are

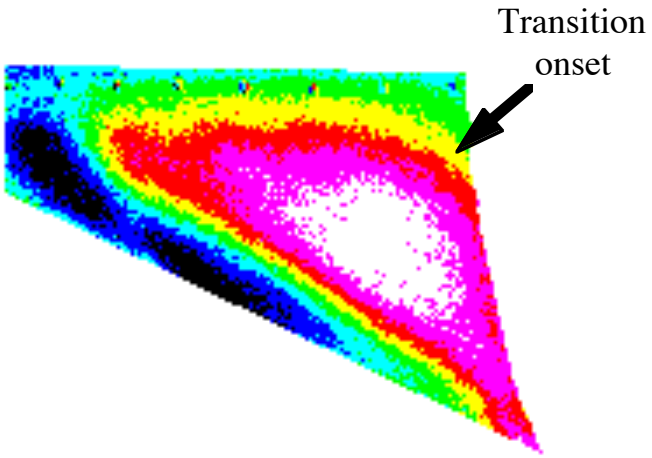

Figure 4. - Transition image of swept-wing model at Mach 3.5.

included in tables: (1) the basic DLT (Eqns. 1 only), (2) DLT with the *L*-constraints (Eqns. 1 and 6), (3) the in-situ calibration including one distortion-correction parameter K_1 as the only one additional unknown and applying the *L*-constraints (Eqns. 2 and 6 with application of Eqn. 10), and (4) a hybrid scheme using

the calibrated values of (x_0, y_0, c) from Eqns. 11, by holding these parameters fixed but still allows some flexibility in allowing the values of appropriate distortion-correction parameters to be obtained in-situ (K_1 only in this example; solving Eqns. 2, 6 and 7). All computations were carried on a Sun SPARC station 2 computer. Note that both algorithms are able to obtain similar results of camera parameters and achieve similar accuracy that is represented either by the relative precision Σ, estimated as $340\sqrt{2}/\max(residual)$, or by the mapping errors at the check points a, b and c. However, the least-squares adjustment algorithm takes much less computer time (*CPU*) to reach the solutions when iteration is required. Some interesting points are noted. First, the *L*-constraints have no significant effects on the solutions. Second, reasonable values are obtained for c in all cases, but the accuracy associated with the principal-point location (x_0, y_0) is poor except for Case 4 in which (x_0, y_0, c) are held fixed at the calibrated values. Third, the accuracy associated with (x_0, y_0, c), computed by Eqns. 7, is improved by including K_1 as shown in Case 3. Because the distortion corrections are proportional to the distance from (x_0, y_0), raised to some power, the errors associated with poor estimates for the principal-point location can be significant even for a camera system with moderate distortion.

Further attempts to improve the accuracy associated with the interior-orientation parameters were tried by solving (x_0, y_0) as additional unknowns, including only one distortion-correction parameter K_1, in photogrammetric mapping by the iterative least-squares adjustment scheme. Results of various combinations of techniques are summarized in Table 2. The *L*-constraints were applied to each case listed in Table 2 even though they do not have significant effect on the solutions. Additional techniques applied to the cases of Table 2 are: (1) the *P*-constraints, (2) the *P*-constraints and a range-limit for (x_0, y_0), (3) the *P*-constraints and *C*-constraints, (4) the *C*-constraints and a range-limit for (x_0, y_0), and (5) the *P*-constraints, *C*-constraints and a range-limit for (x_0, y_0). When the *C*-constraints were applied, the value of the principal distance was given as c = 62.5394 *mm* that was obtained from the Case 3 of Table 1(a). The range-limit for (x_0, y_0) was set as ±1 pixel-dimension, i.e., 54 μm with 2×2 binning, in the neighborhood of the image-plane geometric center. The (x_0, y_0) obtained from iterative solutions are always fallen right on the preset range-limit when it is applied. Therefore, the values of (x_0, y_0) listed in Table 2 were computed by Eqns. 7 in order to be consistent with that shown in Table 1(a). Two important findings must be addressed. First, the results of Case 1 in Table 2 are exactly the same as that of Case 3 in Table 1(a). Although their approaches are different, their procedures are mathematically identical. Second, application of the *C*-constraints and/or a range-limit for (x_0, y_0) improves the accuracy of mapping as denoted by the increases of the relative precision Σ.

Table 1. Results of Photogrammetric Analysis.
(a) Least-Squares Adjustment Algorithm.

Parameter	DLT	Constrained DLT	In Situ *w/* K_1	Hybrid *w/* K_1
x_0 *(mm)*	6.566	6.514	3.320	-0.143
y_0 *(mm)*	-0.736	-0.492	-2.279	0.092
c *(mm)*	58.149	58.214	62.539	63.954
ω *(deg.)*	87.793	88.079	85.460	88.305
ϕ *(deg.)*	46.295	46.356	49.475	52.442
κ *(deg.)*	1.624	1.403	3.407	1.129
X_c *(mm)*	915.563	916.053	955.366	967.815
Y_c *(mm)*	482.545	482.939	515.506	529.822
Z_c *(mm)*	2.340	1.854	0.767	-3.466
K_1 *(mm^{-2})*	-	-	3.957×10^{-5}	5.562×10^{-5}
Σ	57,800	57,600	15,800	45,300
a error (x,y) (μm)	(-31,3)	(-30,3)	(-32,5)	(-31,3)
b error (x,y) (μm)	(14,24)	(14,24)	(15,26)	(16,25)

c error (x,y) (μm)	(12,20)	(12,20)	(13,18)	(12,18)
CPU (sec.)	0.5	0.8	5.4	1.4

(b) Levenberg-Marquardt Algorithm.

Parameter	DLT	Constrained DLT	In Situ *w/* K_1	Hybrid *w/* K_1
x_0 *(mm)*	6.566	6.514	3.957	-0.143
y_0 *(mm)*	-0.736	-0.492	-2.258	0.092
c (mm)	58.149	58.214	62.370	63.954
ω *(deg.)*	87.793	88.079	85.529	88.306
ϕ *(deg.)*	46.295	46.356	48.868	52.441
κ *(deg.)*	1.624	1.403	3.342	1.128
X_c *(mm)*	915.563	916.053	953.821	967.811
Y_c *(mm)*	482.545	482.939	514.632	529.823
Z_c *(mm)*	2.340	1.854	0.764	-3.454
K_1 (mm^{-2})	-	-	4.269×10^{-5}	5.605×10^{-5}
Σ	57,800	57,600	12,200	45,200
a error (x,y) (μm)	(-31,3)	(-30,3)	(-32,5)	(-31,3)
b error (x,y) (μm)	(14,24)	(14,24)	(15,26)	(16,25)
c error (x,y) (μm)	(12,20)	(12,20)	(13,18)	(12,18)
CPU (sec.)	0.5	4.5	150.5	16.2

Table 2. Results of the In-Situ Calibration with Various Improvement Techniques.

Parameter	1. /pc	2. /pc, pplim	3. /pc, /cc	4. /cc, pplim	5. /pc, /cc, pplim
x_0 *(mm)*	3.320	5.268	6.634	2.410	2.657
y_0 *(mm)*	-2.279	-1.660	-1.552	-1.760	-2.878
c (mm)	62.539	60.290	62.539	62.293	62.527
ω *(deg.)*	85.460	86.526	86.529	85.758	84.677
ϕ *(deg.)*	49.475	47.614	46.209	50.390	50.120
κ *(deg.)*	3.407	2.605	2.488	3.237	4.065
X_c *(mm)*	955.366	935.379	955.187	952.669	956.225
Y_c *(mm)*	515.506	499.265	519.916	512.039	514.942
Z_c *(mm)*	0.767	2.408	-0.687	-2.155	1.951
K_1 (mm^{-2})	3.957×10^{-5}	1.872×10^{-5}	6.628×10^{-5}	3.340×10^{-5}	3.091×10^{-5}
Σ	15,800	33,800	3,900	42,200	32,500
a error (x,y) (μm)	(-32,5)	(-44,7)	(-33,6)	(-43,4)	(-39,9)
b error (x,y) (μm)	(15,26)	(15,26)	(15,27)	(13,26)	(15,28)
c error (x,y) (μm)	(13,18)	(16,16)	(13,17)	(14,15)	(17,14)

Note: /pc - with *P*-constraints, /cc - with *C*-constraints, pplim - with range-limit for (x_0, y_0).

Other attempts to include more distortion-correction parameters in the in-situ calibration have been tried. However, all of the results indicated that K_1 is still the most significant parameter and the precision of mapping is deteriorated when more unknowns are involved. These results are not included in the paper.

In all cases described above, the hybridthe transition data. Before mapping the model coordinates scheme of Case 4 of Table 1(a) has the bestto the image plane by Eqns. 2, the optical distortion was relative precision Σ, with the most accuratecalculated by Eqns. 3 with calibrated K_1 and (x_0, y_0). interior-orientation parameters, (x_0, y_0, c). Then, bilinear interpolation was used to determine the Therefore, it is chosen to perform the finalsurface values associated with the calculated pixel photogrammetric mapping. Figure 5 shows thelocations. Checks are made to insure that the mapped data mapping results. A surface grid of the modelfall within the physical boundaries of the CCD array and consisting of 101×101 points was used to mapthe (X, Y, Z) locations of interest are visible.

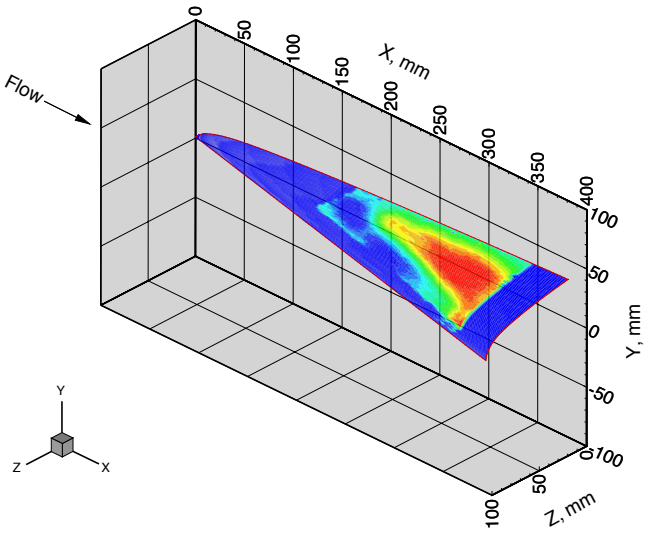

Figure 5. - Photogrammetric mapping of transition image data to CFD grid.

4. SUMMARY

With no prior knowledge of the interior-orientation and distortion-correction parameters, the iterative least-squares adjustment scheme can be used to solve the nonlinear transformation equations with these parameters as additional unknowns. Therefore, the camera is calibrated simultaneously with solving the perspective transformation. This procedure is the so-called in-situ calibration. No special calibration rigs are needed. The computational requirements are easily within the capabilities of modern personal computers, and the algorithms are efficient. The major drawback is that in some cases, the iterative solution may fail to converge to the best solution. There exists a strong correlation between many of the parameters, making it very difficult to solve for the full set of distortion corrections even under the best of circumstances. With only one view of the registration marks, the interior-orientation parameters are very difficult to accurately determine, which further hinders accurate calibration. To circumvent this obstacle, a hybrid scheme is proposed to incorporate the laboratory-calibrated values of interior-orientation parameters in the in-situ calibration. A relative precision of 1 part in 45,300 is achieved in a sample application to luminescent temperature-sensitive paint imaging. However, when there is no laboratory calibration available, various techniques are proposed to improve the accuracy of the in-situ calibration. The best relative precision that can be achieved by the improved in-situ calibration in the same sample application is 1 part in 42,200, that is comparable to the hybrid calibration. This suggests that the in-situ calibration incorporated with the iterative least-squares adjustment scheme is a viable tool for photogrammetric flow visualization.

ACKNOWLEDGMENTS

The author gratefully acknowledges the significant contributions of Dr. Louis N. Cattafesta, III and Mr. Jay G. Moore in developing the TSP imaging techniques and performing the wind-tunnel tests. The author also thanks Dr. Walter L. Snow for his help in the laboratory camera calibration.

REFERENCES

1. Abdel-Aziz, Y. I. and Karara, H. M., "Direct Linear Transformation from Comparator Coordinates into Object Space Coordinates in Close Range Photogrammetry," *Proceedings of the ASP/UI Symposium on Close-Range Photogrammetry*, Urbana, Illinois, pp. 1-18, January 1971.
2. Snow, W. L., Childers, B. A., and Shortis, M. R., "The Calibration of Video Cameras for Quantitative Measurements," *Proceedings of the 39th International Instrumentation Symposium*, Albuquerque, New Mexico, pp. 103-130, May 1993.
3. Bopp, H. and Krauss, H., "Extension of the 11-Parameter Solution for On-the-Job Calibrations of Non-Metric Cameras," *International Archives of Photogrammetry*, vol. 22, no. 5, pp. 7-11, 1978.
4. Cattafesta, L. N. and Moore, J. G., "Review and Application of Non-Topographic Photogrammetry to Quantitative Flow Visualization," AIAA Paper 96-2180, June 1996.
5. Fraser, C. S., "Photogrammetric Camera Component Calibration - A Review of Analytical Techniques," *XVII Congress International Society of Photogrammetry & Remote Sensing*, Washington, D. C., August 1992.
6. Bopp, H. and Krauss, H., "An Orientation and Calibration Method for Non-Topographic Applications," *Photogrammetric Engineering and Remote Sensing*, vol. 44, pp. 1191-1196, 1978.
7. Cattafesta, L. N., "Swept-Wing Suction Experiments in the Supersonic Low-Disturbance Tunnel," High Technology Report No. HTC-9605, High Technology Corporation, June 1996.